MULTIDISCIPLINARY SCIENCE JOURNAL

CONFERENCE PAPER
Published Online: July 12, 2024
https://doi.org/10.31893/multiscience.2024ss0315

Emerging Trends in Engineering and Technology: Shaping the Future of Engineering

Enhancing lubrication performance with novel artificial intelligence-driven film thickness forecasting

Satish Upadhyay[a] ✉ | **Beemkumar Nagappan**[b] | **Awakash Mishra**[c] | **Vaibhav Srivastav**[d]

[a]ATLAS SkillTech University, Mumbai, Maharashtra, Department of uGDX, India.
[b]JAIN (Deemed-to-be University), Ramnagar District, Karnataka, Department of Mechanical Engineering, India.
[c]Maharishi University of Information Technology, Uttar Pradesh, Maharishi School of Engineering and Technology, India.
[d]Vivekananda Global University, Jaipur, Department of Computer Science & Engineering, India.

Abstract Elastohydrodynamic lubrication (EHL) is crucial for the longevity and performance of machine parts subjected to high loads and speeds. Analyzing EHL thickness settings with accuracy is crucial for improving construction and mitigating premature wear. Current approaches for forecasting such variables might be limited in their precision due to computation difficulties. This study presents a novel remora-optimized Gaussian process regression (RO-GPR) approach in calculating the factors related to EHL film dimension, addressing the requirement for a more effective and precise predictive model. The suggested RO-GPR approach is trained and verified by utilizing a dataset that was acquired through methods that are either simulation-based or practical. To show how well the suggested RO-GPR strategy handles the complex structure of EHL mechanisms, its efficacy is compared with that of other approaches. The study's findings reveal that the suggested RO-GPR model can predict EHL film thickness properties with an excellent level of accuracy, indicating its potential as a useful tool for tribological research. By providing insights that can improve the efficiency and construction of machine parts exposed to EHL circumstances, this research advances predictive modeling methodologies for lubrication mechanisms.

Keywords: EHL Film, Machine Parts Thickness, Artificial Intelligence, (RO-GPR)

1. Introduction

Bearing lubrication is accomplished via EHL. Over the past few decades, Theoretical and EHL has been the subject of investigation (Zhang et al., 2017). The majority of machine components operate in mixed EHL environments for industrial applications. It is necessary to investigate the frictional response under hybrid EHL circumstances with the goal of minimizing friction, limit wear and increase machine part lifespan (Gu et al., 2022). The rolling bearing performance is impacted by the load-carrying capability of EHL films. A sufficient amount of lubricant must be supplied to the EHL contact inlet to keep the appropriate film thickness (Li et al., 2018). Numerous parts of lubricated machinery have non-conformal interfaces that can slide and roll together. The EHL settings of these components are caused by the solid surfaces' elasticity deformation (Ewen et al., 2021). The most popular type of gearing for transferring substantial power between non-parallel shafts is spiral bevel gearing, which can scuff, wear and pit as a result of lubricant failure. So, a lot of research investigations have been looking into the lubricating behavior of these gears (Sun et al., 2020). EHL is an exploration of hydrodynamic fluids layer lubricant of elastically flexible structures. Non-conformal linear point contacts are commonly seen to have them yet these include those found in bearings for rolling components and gears (Liu et al., 2021). Wan et al. (2021) created an Ester lubricant anti-wear performance that could be predicted using the Quantitative Structure-Property Relation (QSPR) model. Using the adjacency matrix and molecular graphics, 1444 molecular identifiers with sufficient diversity of each chosen ester molecule were generated. Zhang and Xu (2020) designed the Gaussian method of regression model to illustrate the association between the descriptors of molecules and the initial temperature of the degradation of lubricant additives. Zhao et al. (2021) created a neural network with long and short-term memory to evaluate EHL film profiles instantly and automatically. Furthermore, from optical interferometry picturesa forest model based on neural networks was introduced, which can quickly ascertain the highest and lowest EHL film thickness. Walker et al. (2023) employed lubrication regimens to guarantee the superiority of a training data set while training (ANN) artificial neural networks with data generated by numerical solutions. Next, the EHL main film thickness was predicted using several ANN. Hansen et al. (2021) presented a revised film parameter, $\Lambda*$, that accounts for surface imperfection-induced microscopic EHL effects. The study Zhang et al. (2017) offered a model for predicting the friction of rolling-sliding friction in a variety of lubricating systems such as boundary lubrication, hybrid EHL and complete film lubrication. Zapletal et al. (2018) determined the relationship on the boundary in extremely heavy non-conformal contact

between film thickness and friction, and between full film and mixed lubrication. The goal of Kochi et al. (2017) was to find oil and grease traction besides the thickness of the smooth EHL layer using an optical interferometer or EHL instrument. Zhao et al. (2021) evaluated the micro-textured layer's interface properties at high-load line contact with dimensional hot-line interface EHL and numerical surface creation technologies. Raeymaekers (2021) evaluated the lubricant thickness of layers in patterned hard-on-soft parallel slider bearings using soft EHL simulations. Shirzadegan et al. (2017) proposed a low degree of freedom (LDOF) method to forecast friction in rolling bearings and limited EHL liner contacts, including those that happen between a cam and a roller follower. Jung et al. (2017) implemented numerical analysis to forecast the lubrication areas and film thickness for the thrust ball bearing in several operation scenarios. They discovered that in starved lubrication, the film thickness was influenced by film thinning and replenishment. Zhang et al. (2020) evaluated that an elasto-hydrodynamic (EHD) film activity was affected by the amplitude of the load. A repaired and preset value was varied at different amplitudes by alternating cycles of the load. Šperka et al. (2017) evaluated the variations in film thickness produced by a shallow indentation in a rolling-sliding EHL contacts using amplitude attenuation theory. To enhance the build quality and efficiency of machine parts subjected to EHL conditions, the suggested RO-GPR method improves lubrication mechanism prediction modeling.

The remaining studies pass under the following categories: Section 2 describes solvable analytic proximity equations, Section 3 describes our proposed approach, Section 4 describes our method results and Section 5 concludes the present paper.

2. Solvable Analytic Proximity Equations

The proximity formulas, which belong to the most widely used non-dimensional comparable group, are used to forecast lubricant film properties. The velocity parameter is stated in Equation 1. The material parameter is stated in Equation 2.

$$U = \frac{\eta_0 \cdot v_n}{E' \cdot R} \quad (1)$$

$$G = \alpha_o \cdot E' \quad (2)$$

Thus, the variables are as follows: $v_n$is the speed of absorption, $F_N$is average load, η is the level of viscosity of a fluid, $\alpha_o$is a measure of pressure-viscosity, R is the area of effects. The load parameter is stated in Equation 3.

$$W = \frac{F_N}{E' \cdot R} \quad (3)$$

Equations 4 and 5 provide the parameters for the lowest as well as center film thickness.

$$H_c = \frac{h_c}{R} \quad (4)$$

$$H_{min} = \frac{h_{min}}{R} \quad (5)$$

To ascertain the minimum & central lubricant film thicknesses, this stands for linear regression equations.

2.1. Experimental Design

Statistical designs of experiment methodologies can be used to prepare and assess computer experiments to build an acceptable database to find interactions among variables that are input and output with the least amount of computational work. Designs modified based on the attributes of statistical modeling and numerical simulation can be utilized, in addition to central composite, partial as well as full factorial and Box-Behnken. The production of a wide variety of approximations or meta-models is suitable for the Latin hypercube designing (LHD) or the Latin hypercube samples (LHS) from the evenly spaced test fieldset. Because of this, the distribution of the data points allows them to fill a factor space as equally as possible and despite the large number of factors (n_f), provide information on nearly every part of the element space with minimal processing cost (a small amount of simulationsn_s).

$$x_{ij,LHS} = \frac{x_{ij,LHD} - Z_r[0,1]}{n_s} \quad (6)$$

The resulting LHD, which is a $n_s \times n_f$matrix with arbitrary combinations of the numerals $\{1, 2, 3, .. n_f\}$ inside its column, serves as the foundation for the LHS adjustment. Each LHD element ($x_{ij,LHD}$) is subtracted from one to a random number $Z_r[0,1]$ to get the LHS elements.

The EHL parameters' maximum and minimum values define the intended factor space. Based on typical machine components like rolling bearings or gears that function under tough EHL conditions, these values' ranges were determined. The test field's uniformity of distribution & freedom of correlation can be evaluated using the distances among the data points. For an appropriate and evenly dispersed LHS test field, the minimal distance between each test point was maximized.

$$MaxiMin = \left[\sum_{1 \le I < J \le n_S} d(x_i, x_j)^{-\xi}\right]^{\frac{1}{\xi}} \quad (7)$$

Derived using the application-dependent, positive, integer factor ξ.

2.2. Ehl Modeling

By using the constant-state isothermal Reynolds differential equation, numerical EHL modeling was carried out.

$$\frac{\partial}{\partial x}\left(\frac{\rho \cdot h^3}{12 \cdot \eta}\frac{\partial p}{\partial x}\right) + \frac{\partial}{\partial x}\left(\frac{\rho \cdot h^3}{12\eta}\frac{\partial p}{\partial x}\right) - \frac{\partial}{\partial x}\left(\theta \cdot \rho \cdot h \cdot \frac{u_1+u_2}{2}\right) = 0 \quad (8)$$

Using a slightly altered notation for hydrodynamics, in which $u_1$and $u_2$represent surface velocities, η the viscosity, ρ the weight, p the pressure and h the lubricating layer thickness.

$$\rho(p) = \rho_0 \cdot \left(1 + \frac{0.6 \cdot p}{1+1.7 \cdot p}\right) \quad (9)$$

$$\eta(p) = \eta_0 \cdot e^{[\ln(\eta_0)+9.67]\cdot\left[-1+\left(1+\frac{p}{1.96\times10^8\ pa}\right)^{\frac{\alpha_p \cdot 1.96\times10^8\ pa}{\ln(\eta_0)+9.67}}\right]} \quad (10)$$

This is a crucial need to meet the presumptions used to derive the proximity equations for EHL film thickness.

$$\theta(p) = e^{-\gamma(p).p^2} \quad (11)$$

Where $\gamma(p)$is an algebraic number ξ that is sufficiently high if p is less than zero.

$$h(x,y) = h_0 + \frac{x^2}{2 \cdot R} + \frac{y^2}{2 \cdot R} + \delta \quad (12)$$

The elastic deformation δ, the quadratic estimation of the un-deformed geometry and the rigid body motion $h_0$made up the lubrication gap equation. The latter was computed for an analogous elasticity body with negligible body forces by computing the stable-state linear elasticity equation. When stated in a contract matrix Voigt notation,

$$\nabla[C \cdot \varepsilon_L(U)] = 0 \quad (13)$$

Where, U is the displacement vector, $\varepsilon_L$is a contracted Lagrange small-strain tensor and C is the elasticity matrix of generalized Hooke's law.

$$\delta = |U_z| \quad (14)$$

Additionally, it was expected that the analogous body would be composed of a consistent material that is equal in Young's modulus and it is isotropic.

$$E = \frac{E_1^2 \cdot E_2 \cdot (1+v_2)^2 + E_1 \cdot E_2^2 \cdot (v_1+1)^2}{[F_1 \cdot (1+v_2) + E_2 \cdot (v_1+1)]^{-2}} \quad (15)$$

The hydrodynamic pressure over the contact domain $\Omega_c$was integrally calculated to balance the applied load as a way to maintain force equilibrium.

$$\int_{\Omega_c}^{\Omega e} p dx dy = F_N \quad (16)$$

The pertinent variables were normalized using reference values subscript 0 or Hertzian subscript H to overcome the EHL problem and guarantee appropriate conditioning:

$$W = \frac{x}{b_H}, \Upsilon = \frac{y}{b_H}, p = \frac{p}{p_H}, H = \frac{h \cdot R}{b_H^2}, \bar{\delta} = \frac{\mathrm{h \cdot R}}{\mathrm{b_H^2}}, \bar{\eta} = \frac{\eta}{\eta_0}, \bar{\rho} = \frac{\rho}{\rho_0} \quad (17)$$

The full-system approach created the basis for the numerical solution approach. Initial values were established using the Hertzian concept to determine the first estimate for the elastically deformed solution after reading the inputs.

3. Ai – Based Film Thickness Forecasting

In this section, the integration of the Remora Search Optimization (RSO) and Gaussian Process Regression (GPR) techniques was performed to forecast the EHL film thickness.

3.1. Remora Search Optimization (RSO)

Recently, they developed an optimization technique for swarm intelligence called RSO. The foraging habits of remora acted as the algorithm's model. The remora fish exhibits a behavior known as adsorption, whereby it attaches itself to a host

organism and derives sustenance from the host's resources. Experience will cause it to alternate between the whale and the swordfish. The Whale Optimization Algorithm (WOA) and Sailed Fish Optimization (SFO) algorithms, describe the phases of exploration and exploitation, respectively. In order to obtain food more quickly, there will be concurrent host feeding and empirical attacks amongst various hosts.

3.1.1. Begin over

The first solution of RSO is a set of randomly generated solutions in the search space

$$X_i = lb + rand \times (ub - lb) \quad (18)$$

These are as follows: Xi represents the remora's position; lb, ub, rand stand for the search space's lower as well as upper bounds, respectively besides rand is a random integer between 0 and 1.

3.1.2. Exploration

3.1.2.1. SFO techniques

The remora will stick onto the flag fish and move beside it during the exploring period. The fish's location update formula is derived based on the SFO method.

$$X_j^{t+1} = X_{Best}^t - \left(rand \times \left(\frac{X_{Best}^t + X_{rand}^t}{2}\right) - X_{rand}^t\right) \quad (19)$$

X_{Best}^tDenotes the current optimal remora, $X_{rand}^t$the present state of random memory and t the iteration count,

3.1.2.2. An attempt at experience

During the exploratory phase, a limited set of exploratory strikes will be conducted based on the location of the remora's descendants as well as the host's exact place.

$$X_{att} = X_i^t + \left(X_i^t + X_{pre}\right) \times rand\ n \quad (20)$$

Among these, $rand\ n$ is a number chosen at random with an average range between 0 and 1, $X_{att}$is the fish's tentative attack as well as $X_{pre}$is the location of the fish's last generation.

$$f(\mathrm{X_i^t}) < f(\mathrm{X_{att}}) \quad (21)$$
$$\mathrm{H(i) = round\ (rand)} \quad (22)$$

$H(i)$whose starting value is either 0 or 1, determines which of those is the parasite Remo's host, The whale will provide housing for the remora if $H(i) = 0$ and by the swordfish if $H(i) = 1$. $X_i^t$and X_{att}fitness values are represented by the functions $f(X_i^t)$ and $f(X_{att})$, respectively, as well as round is a rounded function.

3.1.3. Exploitation

3.1.3.1. WOA concept

The remora will connect itself to the whale and travel beside it during the exploitation period. WOA claims that the remora's position update formula is obtained.

$$X_i^{t+1} = D \times e^k \times \cos(2\pi a) + X_i^t \quad (23)$$

$$D = |X_{Best}^t - X_i^t| \quad (24)$$

$$k = rand \times (a - 1) + 1 \quad (25)$$

$$a = -\left(1 + \frac{t}{T}\right) \quad (26)$$

Where T is the largest number of iterations, decreasing linearly with iterations between [−2, 1] and D is the distance from the best position when first updated as well as the current position. *The act of host feeding:* During the exploitation period, the remora fish exhibits a reduced range of movement and conducts localized searches in close proximity to the host.

$$X_i^{t+1} = X_i^t + A \quad (27)$$

$$A = B \times (X_i^t - C \times X_{best}) \quad (28)$$

$$B = 2 \times V \times rand - V \quad (29)$$

$$V = 2 * \left(1 - \frac{t}{T}\right) \quad (30)$$

Where V is used to imitate the fish's value, B is used for simulating the host's value and C is the remora factor, which has a value of 0.1, is applied to limit the fish's position. A represents the remora's traveling distance.

4. Gaussian process regression (GPR)

Using explicit base functions and latent variables such as $f(x_i)$ from the Gaussian process (GP), the GPR stated the outcome. The fundamental operations $h_b(x)$ transferred the input data into a space with p dimensions. A Gaussian-distributed array of random variables, known as a GP, is characterized by its mean $m(x)$and the covariance function $k(x, x')$ which is either hyper-parameterized or kernel parameterized.

$$f(x) \sim GP\ [m(x), k(x, x', \theta_k)] \quad (31)$$

Modeling the GPR response involved utilizing the $p - by - 1$ vectors containing the coefficients of the essential function (β_b) and error variation σ^2.

$$P\left(y_j \middle| f(x_i), x_i\right) \sim N\ (y_i | h(x_i)^T \beta_b + f(x_i), \sigma^2) \quad (32)$$

The kernel function's hyper-parameterθ_k, noise variance σ^2 and base module coefficients $\beta_b$were all computed during training via the built-in MATLAB function "fitrgp."

4.1. Remora search optimized Gaussian process regression (RSO-GPR)

Gaussian process regression and a specific search optimization algorithm are combined in Remora Search Optimized Gaussian Process Regression (RSO-GPR), an advanced machine learning technique. RSO-GPR uses an iterative search procedure to adjust the Gaussian process hyper-parameters in an effort to improve regression tasks efficiency and accuracy. In a variety of mechanical applications, RSO-GPR seeks to maximize performance, minimize friction and improve overall efficiency. This novel approach is a promising development in lubrication science that could have applications in many different engineering and industrial fields. The suggested Remora search optimized Gaussian process regression RSO-GPR technique is displayed in pseudo code 1.

Pseudo code 1 Remora search optimized Gaussian process regression (RSO-GPR)

```
Step 1: Initialize Gaussian Process Regression model
gprModel = fitrgp(X_train, y_train, 'KernelFunction', 'squared exponential');
Step 2: Define the objective function for optimization
objFunction = @(hyperparameters) crossval('mse', X_train, y_train, ...
'Predfun', @(X_train, y_train, X_test, hyperparameters) ...
predict(fitrgp(X_train, y_train, 'KernelFunction', 'squaredexponential', ...
'KernelParameters', hyperparameters), X_test), 'Kfold', 5);
Step 3: Perform optimization using fminsearch
initialHyperparameters = gprModel.KernelInformation.KernelParameters;
optimizedHyperparameters = fminsearch(objFunction, initialHyperparameters);
Step 4: Update GPR model with optimized hyperparameters
updatedGPRModel = fitrgp(X_train, y_train, 'KernelFunction', 'squaredexponential', ...
'KernelParameters', optimizedHyperparameters);
Step 5: Predict using the test set.
predictions = predict(updatedGPRModel, X_test);
Step 6: Evaluate the performance of the model
mse = mean((predictions - y_test).^2);fprintf('Mean Squared Error on Test Set: %.4f\n', mse);
```

5. Results

We make use of data gathered from full-system finite-element (FE) solution-based EHL simulations (Zhao et al., 2023).

5.1. Setting up for experimentation

Tasks were carried out on a laptop with an Intel i7 10th Gen processor and 32 GB RAM, running Windows 10 and MATLAB R2023b. With this configuration, software capabilities were combined with strong hardware performance to ensure effective task execution and analysis. In the result section, we evaluated some outcome indicators, encompassing the R-squared (R^2), mean absolute errors (MAE) and roots of mean square errors (RMSE).

Existing technologies such as Random Forest (RF) (Sharma et al., 2020) generalized linear model (GLM) (Sharma et al., 2020) and decision tree (DT) (Sharma et al., 2020) have been utilized. Measuring the average absolute variance among estimated and actual values is the Mean Absolute Error (MAE). Results of the MAE are shown in Figure 1 and Table 1. It generated values of (31.21), (19.73) and (38.05) for (DT), (RF) and (GLM) in that order. At an average MAE of (11.36), the suggested method, called RSO-GPR, produced better results. It shows how much better our suggested RSO-GPR approach performs.

Table 1 Results of the mean absolute error.

Methods	MAE
DT (Sharma et al., 2020)	31.218
RF (Sharma et al., 2020)	19.739
GLM (Sharma et al., 2020)	38.059
RSO-GPR (Proposed)	11.369

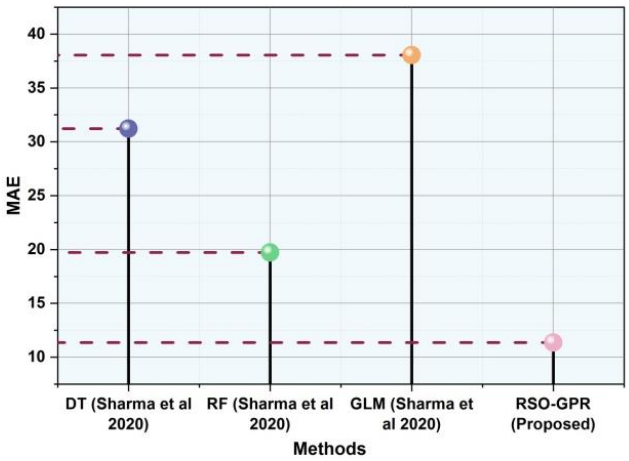

Figure 1 The mean absolute error result.

To quantify the average amount of errors among predicted along with actual values and give a numerical assessment of the strategy accuracy, in statistics, the Root Mean Squared Error (RMSE) measure is employed. Results for the RMSE are displayed in Table 2 and Figure 2. It produced values for (DT), (RF) as well as (GLM) of (36.87), (27.61) and (41.19) in that order. The suggested method, named RSO-GPR, produced better results, with an average RMSE of (20.48).

Table 2 Results of the root mean square error.

Methods	RMSE
DT (Sharma et al., 2020)	36.877
RF (Sharma et al., 2020)	27.619
GLM (Sharma et al., 2020)	41.195
RSO-GPR (Proposed)	20.485

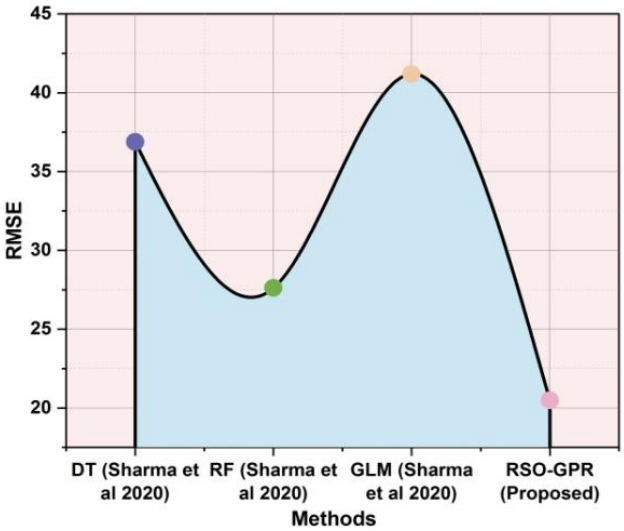

Figure 2 The RMSE result.

It demonstrates a significant improvement in the performance of our proposed RSO-GPR method. The amount of variability in the dependent variable that can be attributed to an independent variable is measured by R-squared (R^2). Higher values suggest a better fit. The range is 0 to 1. The R^2 results are shown in Figure 3 and Table 3. It generated values of (0.918), (0.946) and (0.929) for (DT), (RF) and (GLM), in that order. Better outcomes were obtained with the recommended approach, known as RSO-GPR, with an R^2 value of (0.968). It shows our suggested RSO-GPR method's performance is effective.

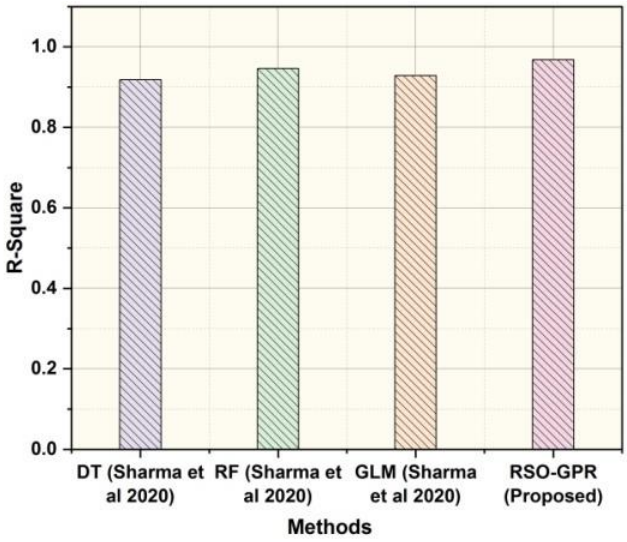

Figure 3 The outcome of R-squared (R^2).

Table 3 Results of the R-squared (R^2).

Methods	R-Square
DT (Sharma et al., 2020)	0.918
RF (Sharma et al., 2020)	0.946
GLM (Sharma et al., 2020)	0.929
RSO-GPR [Proposed]	0.968

6. Conclusion

This study presents a novel remora-optimized Gaussian process regression (RO-GPR) approach to identify the factors connected to EHL film dimension. The proposed RSO-GPR methodology is trained and validated on a dataset obtained by simulation-based methodologies. The proposed methodology was implemented with MATLAB R2023b. The effectiveness of proposed RSO-GPR strategy is contrasted with alternative methods to demonstrate how it manages the intricate structure of EHL processes. In order to assess the parameters such as MAE, RMSE and R^2, our suggested methodology is superior to existing methods, the calculated values for RMSE, MAE and R^2 were 20.48, 11.36 and 0.968, respectively. There are several obstacles to improve lubrication performance with an AI-driven film thickness forecasting system, including insufficient training data and privacy issues. In the future, improving training data quality, addressing privacy issues, fine-tuning models for wider applicability as well as implementing explainable AI approaches will be necessary to overcome these difficulties in AI-driven lubricant forecasts that promote greater confidence and accessibility.

Ethical considerations

Not applicable.

Conflict of Interest

The authors declare no conflicts of interest.

Funding

This research did not receive any financial support.

References

Allen, Q., & Raeymaekers, B. (2021). Soft EHL simulations of lubricant film thickness in textured hard-on-soft bearings considering different cavitation models, in the context of prosthetic hip implants. *Tribology Letters, 69*, 1-17. https://doi.org/10.1007/s11249-021-01498-8

Ewen, J. P., Spike, H. A., & Dini, D. (2021). Contributions of molecular dynamics simulations to elastohydrodynamic lubrication. *Tribology Letters, 69*(1), 24. https://doi.org/10.1007/s11249-021-01399-w

Gu, C., Zhang, D., Jiang, X., Meng, X., Wang, S., Ju, P., & Liu, J. (2022). Mixed EHL problems: An efficient solution to the fluid–solid coupling problem with consideration of elastic deformation and cavitation. *Lubricants, 10*(11), 311. https://doi.org/10.3390/lubricants10110311

Hansen, J., Björling, M., & Larsson, R. (2021). A new film parameter for rough surface EHL contacts with anisotropic and isotropic structures. *Tribology Letters, 69*(2), 37. https://doi.org/10.1007/s11249-021-01411-3

Jung, S., Lee, B., Yu, Y., & Cho, Y. (2017). A study on the change in the film thickness of ball bearing in starved EHL. *Tribology and Lubricants, 33*(3), 119-125. https://doi.org/10.9725/kstle.2017.33.3.119

Kochi, T., Ichimura, R., Yoshihara, M., Dong, D., & Kimura, Y. (2017). Film thickness and traction in soft EHL with grease. *Tribology Online, 12*(4), 171-176. https://doi.org/10.2474/trol.12.171

Li, X., Guo, F., Wong, P., & Zhao, Y. (2018). Regulation of lubricant supply by wettability gradient in rolling EHL contacts. *Tribology International, 120*, 565-574. https://doi.org/10.1016/j.triboint.2018.01.020

Liu, Zhang, B., Schneider, V., Venner, C. H., & Poll, G. (2021). Two-dimensional generalized non-Newtonian EHL lubrication: Shear rate-based solution versus shear stress-based solution. *Proceedings of the Institution of Mechanical Engineers, Journal of Engineering Tribology, 235*(12), 2626-2639. https://doi.org/10.1177/13506501211050484

Sharma, G., Kotia, A., Ghosh, S. K., Rana, P. S., & Bawa, S. (2020). Kinematic viscosity prediction of nanolubricants employed in heavy earth moving machinery using machine learning techniques. *International Journal of Precision Engineering and Manufacturing, 21*, 1921-1932. https://doi.org/10.1007/s12541-020-00379-9

Shirzadegan, M., Larsson, R., & Almqvist, A. (2017). A low degree of freedom approach for prediction of friction in finite EHL line contacts. *Tribology International, 115*, 628-639. https://doi.org/10.1016/j.triboint.2017.06.019

Šperka, P., Křupka, I., & Hartl, M. (2017). Prediction of shallow indentation effects in a rolling-sliding EHL contact based on amplitude attenuation theory. *Tribology Online, 12*(1), 1-7. https://doi.org/10.2474/trol.12.1

Sun, X., Liu, Y., Zhao, Y., & Liu, M. (2020). EHL analysis of spiral bevel gear pairs considering the contact point migration due to deformation under load. *Mathematical Problems in Engineering, 2020*. https://doi.org/10.1155/2020/2047876

Walker, J., Questa, H., Raman, A., Ahmed, M., Mohammadpour, M., Bewsher, S. R., & Offner, G. (2023). Application of tribological artificial neural networks in machine elements. *Tribology Letters, 71*(1), 3. https://doi.org/10.1007/s11249-022-01673-5

Wan, Z., Wan, Q., Liu, D., & Liang, J. (2021). Discovery of ester lubricants with low coefficient of friction on material surface via machine learning. *Chemical Physics Letters, 773*, 138589. https://doi.org/10.1016/j.cplett.2021.138589

Zapletal, T., Šperka, P., Křupka, I., & Hartl, M. (2018). The effect of surface roughness on friction and film thickness in transition from EHL to mixed lubrication. *Tribology International, 128*, 356-364. https://doi.org/10.1016/j.triboint.2018.07.047

Zhang, X., Glovnea, R., Morales-Espejel, G., & Félix-Quiñonez, A. (2020). The effect of working parameters upon elastohydrodynamic film thickness under periodic load variation. *Tribology Letters, 68*, 1-10. https://doi.org/10.1007/s11249-020-01303-y

Zhang, X., Li, Z., & Wang, J. (2017). Friction prediction of rolling-sliding contact in mixed EHL. *Measurement, 100*, 262-269. https://doi.org/10.1016/j.measurement.2017.01.005

Zhang, Y., Wang, W., Zhang, S., & Zhao, Z. (2017). Experimental study of EHL film thickness behaviour at high speed in ball-on-ring contacts. *Tribology International, 113*, 216-223. https://doi.org/10.1016/j.triboint.2023.108353

Zhang, Y., & Xu, X. (2020). Machine learning decomposition onset temperature of lubricant additives. *Journal of Materials Engineering and Performance, 29*, 6605-6616. https://doi.org/10.1007/s11665-020-05146-5

Zhao, J., Li, Z., Zhang, H., & Zhu, R. (2021). Prediction of contact and lubrication characteristics of micro-textured surface under thermal line contact EHL. *Frontiers in Mechanical Engineering, 7*, 672588. https://doi.org/10.3389/fmech.2021.672588

Zhao, Y., Deng, Z., & Cheng, Z. (2023). Automatic EHL film measurement via a long short-term memory neural network and neural network forest. *Tribology International, 182*, 108353. https://doi.org/10.1016/j.triboint.2023.108353